Dalton Transactions

Accepted Manuscript

ROYAL SOCIETY OF CHEMISTRY

www.rsc.org/dalton

Graphical abstract

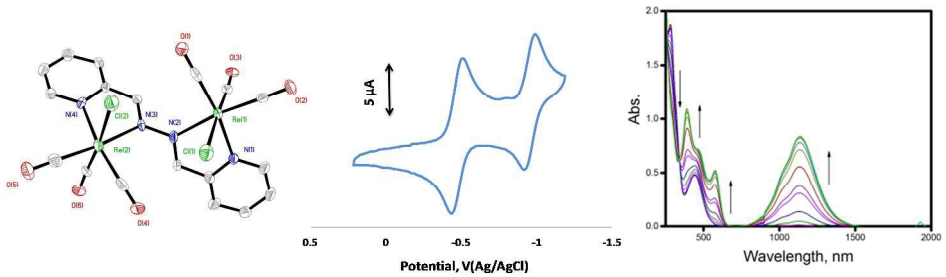

We present two strongly coupled $Re(CO)_3$ dimers, where the metals are linked via a bis-hydrazine Schiff base ligand as well as their monomeric analogs. Strong coupling between the ligand based orbitals the dimers is observed as measured by reductive cyclic voltammetry: ~480 mV separations between sequential reductions that correspond to comproportionation constants close to 1.5×10^8.

Journal Name

ARTICLE

Hydrazine-mediated strongly coupled $Re(CO)_3$ dimers

A. Hasheminasab,[a] H. M. Rhoda,[b] L.A. Crandall,[a] J.T. Ayers,[c] V.N. Nemykin,[b]* R. S. Herrick,[c]* C. J. Ziegler[a]*

Received 00th January 20xx,
Accepted 00th January 20xx

DOI: 10.1039/x0xx00000x

www.rsc.org/

Dimeric metal complexes can often exhibit coupling interactions via bridging ligands. In this report, we present two $Re(CO)_3$ dimers, where the metals are linked via a bis(pyca) hydrazine (pyca = pyridine-2-carbaldehyde imine) Schiff base ligand. For the dimeric compounds **4** and **5**, we observe strong coupling across the dimer as measured by cyclic voltammetry: ~480 mV separations between the first and the second reduction waves that correspond to comproportionation constants close to 1.5×10^8. Evidence for a mixed valence state upon one electron reduction was also observed by spectroelectrochemistry in which a clear inter-valence charge-transfer (IVCT) band was observed in [**4**]- and [**5**]- complexes. The electronic structures of all target compounds were probed by DFT and TDDFT computational methods. DFT calculations indicate that reduction takes place at the diimine units, and that the observed coupling is a ligand-based phenomenon, rather than one that involves metal-based orbitals.

Introduction

Dimeric $Re(CO)_3$ compounds have been attracting interest as synthetic targets, both as components of materials and for possible biological applications.[1–7] There are many examples of $Re(CO)_3$ dimers where the two metal ions are bridged by halides, hydroxides or alkoxides, organic fragments (such as a phenyl ring) or by nitrogenous ligands. A variety of experimental and theoretical studies have been carried out to probe the effects of dimer structure on physical properties, such as photophysics or electron transfer.[3,8–23] Under certain conditions, $Re(CO)_3$ complex centers can couple through a bridging ligand. Parameters including bridge type, metal-metal distance, interplanar distances, degree of saturation, conjugation, and orientation of the bridge moiety can all affect the degree of coupling and their resultant properties such as redox potentials.[7,12,14,15,18,24–27]

Rhenium(I) diimines have been studied for their photochemical activities, due to the presence of metal-to-ligand charge transfer bands in these compounds. Irradiation of $Re(CO)_3$ diimines can be used to initiate chemical reactions or to induce electron transfer processes. Coupled photochemically-active transition metal compounds can be used as components of materials; these have been employed with several d^6 metal ion systems. Although the electronic interactions of metals such as ruthenium have been extensively explored in dimeric complexes, similar experiments have not been carried out on $Re(CO)_3$ diimine systems. In this report, we present the synthesis and characterization of two $Re(CO)_3$ dimeric compounds that exhibit an extraordinary

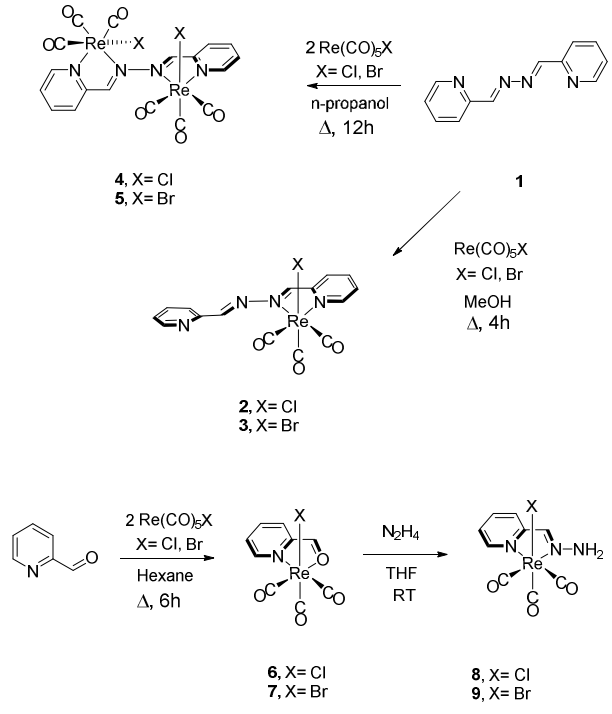

Scheme 1

[a] Department of Chemistry, University of Akron, OH 44325-3601, USA
[b] Department of Chemistry & Biochemistry, University of Minnesota Duluth, Duluth, MN 55812, USA
[c] Department of Chemistry, College of the Holy Cross, Box C, Worcester, MA 01610-2395, USA

Electronic Supplementary Information (ESI) available: Spectroscopic results, electrochemical experiments, X-ray structural data and calculations. Crystallographic data for the structures 3-5, 8, 9 have been deposited with the Cambridge Crystallographic Data Centre as cif files (CCDC 1414734-1414738) Copies of these data can be obtained free of charge via www.ccdc.cam.ac.uk/conts/retrieving.html or from the Cambridge Crystallographic Data Centre, 12, Union Road, Cambridge CB21EZ, UK (fax: (+44) 1223-336-033; Email: deposit@ccdc.cam.ac.uk). See DOI: 10.1039/x0xx00000x

degree of coupling across the dimers. The coupling can be readily observed via cyclic voltammetry and spectroelectrochemistry, which show a large separation between sequential reduction waves and the presence of an apparent inter-valence charge transfer (IVCT) band, respectively. We also present several monomeric analogues and monometalated compounds which we can use as controls to study the specific effects of metal dimer structures on electronic properties. DFT and TDDFT calculations reveal that the reductions are primarily ligand-based rather than metal-centered, which is in agreement with the literature on the reduction of monomeric $Re(CO)_3$ bipyridine complexes.

Experimental

General information

Materials and Methods: Reagents were purchased from Strem, Acros Organics, TCI America or Sigma-Aldrich and used as received without further purification. Syntheses were performed to minimize exposure to air or water. All solvents were dried and deoxygenated by alumina and copper columns in the Pure Solv solvent system (Innovative Technologies, Inc.); dried solvents were stored over molecular sieves.

NMR spectra were recorded on Varian Mercury 300 MHz and 500 MHz instruments. Chemical shifts were reported with respect to residual solvent peaks as internal standard (^{1}H: d_6-DMSO, δ = 2.50 ppm; ^{13}C: d_6-DMSO, δ = 39.7 ppm). Infrared spectra were collected on Thermo Scientific Nicolet iS5 which was equipped with iD5 ATR. Electronic absorption spectra were recorded on Hitachi U-2000 UV-vis spectrophotometer. Elemental Analyses were performed by Atlantic Microlab of Norcross, GA 30091. Mass Spectrometric analyses were carried out at the Mass Spectrometry center at The University of Akron in Akron, OH.

X-ray Data Collection and Structure Determination: X-ray intensity data for compounds **3** and **9** were measured at 100 K on a CCD-based X-ray diffractometer system equipped with a Mo-target X-ray tube (Mo Kα radiation, λ = 0.71073 Å) operated at 2000 W power. Data for **4**, **5** and **8** were collected on a CCD-based diffractometer with dual Cu/Mo ImuS microfocus optics (Cu Kα radiation, λ = 1.54178 Å). Crystals were mounted on a cryoloop using Paratone oil and placed under a steam of nitrogen at 100 K. The detector was placed at a distance of 5.009 cm from the crystal. Crystals data and structure refinement parameters are summarized in Table **1**.

Cyclic Voltammetry: Cyclic voltammograms were obtained using a standard three electrode cell and Electrochemical analyzer BAS 100B from Bioanalytical systems and were recorded at 298 K under the following conditions: 10^{-3} M samples in dimethylformamide (DMF) in the presence of 0.1 M tetrabutylammonium hexafluorophosphate ($TBAPF_6$) or tetrabutylammonium perchlorate (TBAP) as a supporting electrolyte, Ag/Ag^+ reference electrode, 0.79 mm^2 gold working electrode, and platinum wire auxiliary electrode. The working electrode was polished first with 3 µm fine diamond, then 0.05 µm alumina. The electrode was rinsed with ethanol and deionized water after each polishing and wiped with a Kimwipe. The non-aqueous Ag/Ag^+ reference electrode was prepared by soaking the silver wire in the degassed DMF solution of 0.01M $AgClO_4$: 0.1M $TBAPF_6$. Approximated formal potentials for a reversible redox couples ($E^{\circ\prime}= (E_{pc} + E_{pa})/2$) were all referenced against Ag/Ag^+. $\Delta E_p = E_{pa} - E_{pc}$, $\Delta E = (E_1^{\circ\prime} - E_2^{\circ\prime})$ and peak currents were calculated by use of an extrapolated baseline current[28,29] Potentials were reported against Ag/AgCl reference electrode and compared with previous data reported by Geiger and coworker.[30] The linear dependence between the square root of the scan rate ($v^{1/2}$) and both the cathodic (i_{pc}) and anodic (i_{pa}) currents was examined between 0.1 to 0.5 V/s, and the formal potentials are independent of scan rate. At a 0.10 V/s sweep rate, the FcH/FcH^+ occurs at 0.48 ±0.005 V (ΔE_p = 71mV; i_{pa}/i_{pc} = 1.02).

Spectroelectrochemistry: Spectroelectrochemical data were collected on a JASCO-720 spectrophotometer at room temperature. The experiments were conducted using a CHI-620C electrochemical analyzer using a custom-made 1 mm cell with a platinum mesh-working electrode. In order to suppress overtones in the NIR region of the optical spectra, measurements were conducted in 0.3 M TBAP in DMF.

DFT and TDDFT calculations: The starting geometries of all compounds were taken from X-ray structures. They were optimized using the B3LYP exchange-correlation functional[31,32] coupled with the relativistic DZP basis set for the Re atom[33] and the 6-311G(d)[34] basis set for the remaining atoms. Energy minima in optimized geometries were confirmed by frequency calculations. DMF was used as a solvent in all of the single point DFT-PCM and TDDFT-PCM calculations; solvent effects were calculation using the polarized continuum model (PCM).[35] The first 30 states of each compound were calculated in all TDDFT-PCM calculations. All DFT calculations were conducted using the Gaussian 09 software package,[36] and the QMForge program[37] was used for the molecular orbital analysis.

Synthetic procedures

Synthesis of 1, 2-pyridinecarboxaldehydeazine, (pyca-pyca, pyca = pyridine-2-carbaldehyde imine). This compound was prepared as previously described.[38]

Synthesis of 2 and 3 [Re(CO)3(pyca-pyca)X; 2, X = Cl; 3 = Br]. The procedure for the synthesis of **2** is representative for both compounds. **2**: $Re(CO)_5Cl$ (0.050 g, 0.141 mmol) and **1** (0.030 g, 0.141 mmol) were refluxed in 25 mL of methanol for 4 h. After cooling to room temperature, a red solid was filtered and washed with 10 mL hexane. Crystals suitable for X-ray diffraction were prepared by slow vapor diffusion of water into a DMSO solution. Yield: 52 mg (71%). ^{1}H NMR (500 MHz, d_6-DMSO, δ (ppm)): 9.40 (s, 1H, metal-bound N=C*H*), 9.07 (d, J = 4.5Hz, 1H, H on metal-bound py), 8.86 (s, 1H, N=C*H*), 8.81 (d, J = 5.0Hz 1H, H on metal-bound py), 8.35 (m, 2H, on metal bound and free py), 8.20 (d, J = 8.0Hz, 1H, on free py), 8.05 (m, 1H, H on metal bound py), 7.84 (m, 1H, H on metal-bound py), 7.65 (m, 1H, H on metal-bound py) ppm. ^{13}C NMR (75 MHz d_6-DMSO, δ (ppm)) 196.8, 186.0, 165.0, 163.4, 153.5, 153.4, 150.5, 150.0, 140.6, 137.7, 130.1, 129.7, 127.0, 122.6 ppm.

CHN Anal. Calc. for $Re_1C_{15}H_{10}O_3N_4Cl_1$: C, 34.92; H, 1.95; N, 10.85. Found: C, 35.11; H, 2.06; N, 10.69. IR (CO stretch, cm^{-1}): 2020, 1888. MS (ESI): m/z = calc. for $Re_1C_{15}H_{10}O_3N_4Cl_1Na$: 538.98 found 539.0. UV-Vis spectrum in CH_2Cl_2 λ_{max} 314 nm ($\varepsilon = 1.7 \times 10^4$ M^{-1} cm^{-1}) and λ_{max} 437 nm ($\varepsilon = 2.6 \times 10^2$ M^{-1} cm^{-1}).

3: Yield: 34 mg (48%). ^{1}H NMR (500 MHz, d_6-DMSO, δ (ppm)): 9.40 (s, 1H, metal-bound N=C*H*), 9.09 (d, J = 5.0 Hz, 1H, H on metal-bound py), 8.87(s, 1H, N=C*H*), 8.81(d, J = 4.5Hz 1H, H on metal-bound py), 8.35(m, 2H, on metal bound and free py), 8.19 (d, J = 8.0Hz, 1H, on free py), 8.05 (m, 1H, H on metal bound py), 7.83(m, 1H, H on metal-bound py), 7.65 (m, 1H, H on metal-bound py) ppm. ^{13}C NMR (75 MHz d_6-DMSO, δ (ppm)) 196.8, 165.1, 163.4, 153.5, 153.4, 150.5, 150.0, 140.6, 137.7, 130.1, 129.7, 127.0, 122.6 ppm. CHN Anal. Calc. for $Re_1C_{15}H_{10}O_3N_4Br_1$: C, 32.15; H, 1.79; N, 9.99. Found: C, 32.04; H, 1.82; N, 9.73. IR (CO stretch, cm^{-1}): 2021, 1893. MS (ESI): m/z = calc. for $Re_1C_{15}H_{10}O_3N_4Br_1Na$: 582.93 found 582.9. UV-Vis spectrum in CH_2Cl_2 λ_{max} 310 nm ($\varepsilon = 1.7 \times 10^4$ M^{-1} cm^{-1}) and λ_{max} 433 nm ($\varepsilon = 2.7 \times 10^2$ M^{-1} cm^{-1}).

Synthesis of 4 and 5 [Re(CO3)X(pyca-pyca)Re(CO)3X; 4, X = Cl; 5 = Br]. The procedure for the synthesis of **4** is representative for both compounds. **4**: $Re(CO)_5Cl$ (0.050 g, 0.141 mmol) and **1** (0.015 g, 0.0705 mmol) were refluxed in 25 mL of *n*-propanol for 12 h. After cooling to room temperature, a dark red solid was filtrated and washed with 10 mL hexane. Yield: 47 mg (82 %).Crystals suitable for X-ray diffraction were prepared by slow vapor diffusion of water into a DMSO solution. ^{1}H NMR (300 MHz, d_6-DMSO, δ (ppm)): 9.58 (d, 2H, N=C*H*), 9.10 (d, J = 6.0Hz, 2H, H on py), 8.72 (d, J = 6.0Hz, 2H, H on py), 8.44 (m, 2H, H on py), 7.95 (m, 2H on py).^{13}C NMR (75 MHz d_6-DMSO, δ (ppm)) 196.6, 195.8, 186.0, 167.3, 165.51, 154.17, 153.82, 151.7, 151.5, 141.0, 140.8, 132.1, 131.9, 131.0 ppm. CHN Anal. Calc. for $Re_2C_{18}H_{10}O_6N_4Cl_2$: C, 26.31; H, 1.22; N, 6.82. Found: C, 26.25; H, 1.25; N, 6.72. IR (CO stretch, cm^{-1}): 2020, 1885. MS (ESI): m/z = calc. for $Re_2C_{18}H_{10}O_6N_4Cl_2Na$: 844.90 found 844.9. UV-Vis spectrum in CH_2Cl_2 λ_{max} 293 nm ($\varepsilon = 2.0 \times 10^4$ M^{-1} cm^{-1}) and λ_{max} 458 nm ($\varepsilon = 6.0 \times 10^3$ M^{-1} cm^{-1}).

5: Yield 42 mg (75%). ^{1}H NMR (300 MHz, d_6-DMSO, δ (ppm)): 9.57 (d, 2H, N=C*H*), 9.1 (d, J = 6.0Hz, 2H, H on py), 8.74 (d, J = 6.0Hz, 2H, H on py), 8.42 (m, 2H, H on py), 7.94 (m, 2H on py).^{13}C NMR (75 MHz, d_6-DMSO, δ (ppm)): 195.9, 195.7, 185.4, 167.2, 165.2, 154.2, 153.9, 151.6, 151.4, 140.8, 140.6, 132.2, 132.0, 130.0. CHN Anal. Calc. for $Re_2C_{18}H_{10}O_6N_4Br_2$: C, 23.74; H, 1.11; N, 6.15. Found: C, 24.00; H, 1.09; N, 6.03. IR (CO stretch, cm^{-1}): 2014, 1913, and 1880. MS (ESI): m/z = calc. for $Re_2C_{18}H_{10}O_6N_4Br_2Na$: 932.79 found 932.8. UV-Vis spectrum in CH_2Cl_2 λ_{max} 289 nm ($\varepsilon = 2.0 \times 10^4$ M^{-1} cm^{-1}) and λ_{max} 470 nm ($\varepsilon = 5.4 \times 10^3$ M^{-1} cm^{-1}).

Synthesis of 8 and 9 [Re(CO3)X(pyca-NH2); 8, X = Cl; 9 = Br]. The procedure for the synthesis of **8** is representative for both compounds.

8: $Re(CO)_5Cl$ (0.050 g, 0.141 mmol) and pyridine-2-carboxaldehyde (0.0151 g, 0.141 mmol) were refluxed in 25 mL of hexane for 6 h. A red solid (6) was filtered and washed with diethyl ether. The solid was then dissolved in THF and hydrazine monohydrate (0.0070 g, 0.141 mmol) was added under vigorous stirring. The yellow solid was filtered and washed with 25 mL diethyl ether. Crystals suitable for X-ray diffraction were prepared by slow vapor diffusion of hexane into a $CHCl_3$ solution. Yield 48 mg (80%). ^{1}H NMR (300 MHz, d_6-DMSO, δ (ppm)): 8.78 (d, J = 6.0Hz, 1H, H on py), 8.41 (s, 2H, H on $–NH_2$), 8.34 (s, 1H, N=C*H*), 8.11 (m, 1H, H on py), 7.90 (d, J = 9.0 Hz, 1H on py), 7.48 (m, 1H, H on py).^{13}C NMR (75 MHz d_6-DMSO) 197.6, 196.0, 188.4, 155.9, 151.9, 141.7, 139.6, 125.2, 124.4 ppm. CHN Anal. Calc. for $Re_1C_9H_7O_3N_3Cl_1$: C, 25.32; H, 1.65; N, 9.84. Found: C, 25.47; H, 1.80; N, 9.77. IR (CO stretch, cm^{-1}): 2025, 1892. MS (ESI): m/z = calc. for $Re_1C_9H_7O_3N_3Cl_1Na$: 450.00 found 449.8. UV-Vis spectrum in CH_2Cl_2 λ_{max} 296 nm ($\varepsilon = 8.6 \times 10^3$ M^{-1} cm^{-1}) and λ_{max} 388 nm ($\varepsilon = 3.5 \times 10^3$ M^{-1} cm^{-1}).

9: Yield 36 mg (61 %). ^{1}H NMR (300 MHz, $CDCl_3$, δ (ppm)): 8.92 (d, 1H, J = 5.5Hz, H on py), 8.18 (s, 1H, N=C*H*), 8.95 (m, 1H, H on py), 7.65 (d, J = 7.5Hz, 1H on py), 7.42(m, 1H, H on py), 6.54 (s, 2H, H on $–NH_2$). CHN Anal. Calc. for $Re_1C_9H_7O_3N_3Br_1$: C, 22.93; H, 1.49; N, 8.91. Found: C, 22.52; H, 2.05; N, 8.95. IR (CO stretch, cm^{-1}): 2019, 1873. MS (ESI): m/z = calc. for $Re_1C_9H_7O_3N_3Br_1Na$: 493.91 found 493.8. UV-Vis spectrum in CH_2Cl_2 λ_{max} 296 nm ($\varepsilon = 8.2 \times 10^3$ M^{-1} cm^{-1}) and λ_{max} 393 nm ($\varepsilon = 2.9 \times 10^3$ M^{-1} cm^{-1}).

Results and Discussion

In an earlier report,[39] we outlined the one-pot synthesis of a series of phenylene-bridged dinuclear Re(I) complexes, as well as their structures, spectroscopic features and electrochemical properties. These compounds could be readily synthesized via the reaction of phenylene diamines, pyridine-2-carboxyaldehyde and $Re(CO)_5X$ (X = Cl, Br). We surmised that we could generate "phenylene-free" analogs via the reaction of hydrazine and pyridine-2- carboxyaldehdye. This reaction, shown in Scheme 1, affords a bis-Schiff base diazine ligand (compound **1**) which can coordinate one or two equivalents of $Re(CO)_3$ and can be considered structurally similar to the phenylene-bridged ligands that we reported previously. This allowed us to not only generate the desired dimeric compounds **4** and **5**, but also the monomeric species **2** and **3**. Compound **2** was reported previously.[40] The degree of metalation was controlled by the choice of solvent; the higher boiling alcohol, *n*-propanol, afforded the bis-metalated species, but reaction in methanol resulted in the formation of only the singly-metalated product. The monometalated products **2** and **3** can be used as controls to determine the effect of dimeric coupling on the properties of **4** and **5**. We also synthesized alternative monomeric analogues to **4** and **5,** $Re(CO)_3$ diimine with a terminal amine group. Compounds **8** and **9**, can be produced from pyridine-2-carboxyaldehyde and an excess of hydrazine by first forming the rhenium pyridine-2-carboxaldehyde adducts **6** and **7** *in situ*, [41,42] followed by addition of hydrazine (Scheme 1).

All new compounds synthesized for this study were fully characterized, including via X-ray crystallography. Figure 1 shows the structures of the bromide compounds (**3**, **5**, and **9**); the chloride analogs **2**, **4**, and **8** effectively have nearly identical structures (see Supplementary Information). The compounds exhibit the expected facial $Re(CO)_3$ coordination

Compound	**3**	**4**	**5**	**8**	**9**
Empirical formula	$C_{15}H_{10}BrN_4O_3Re$	$C_{18}H_{10}Cl_2N_4O_6Re_2$	$C_{18}H_{10}Br_2N_4O_6Re_2$	$C_9H_7BrClN_3O_3Re$	$C_9H_7BrClN_3O_3Re$
Formula weight	560.38	821.60	910.52	426.83	471.29
Crystal system	Triclinic	Monoclinic	Triclinic	Monoclinic	Triclinic
Space group	P-1	P2/c	P-1	P2(1)	P-1
a/ Å	7.036(3)	14.4660(9)	11.4508(7)	6.4068(3)	6.477(3)
b/ Å	9.082(4)	11.4063(8)	11.8036(7)	8.8341(5)	8.265(3)
c/ Å	7.036(3)	12.9730(10)	11.8641(7)	14.4493(8)	12.881(5)
α(°)	81.144(4)	90	75.213(4)	90	95.607(4)
β(°)	84.259(4)	96.727(5)	67.040(3)	101.947(3)	93.095(4)
γ(°)	72.527(4)	90	65.574(4)	90	97.211(4)
Volume ($Å^3$)	801.9(6)	2125.9(3)	2084.2(2)	800.09(7)	679.3(5)
Z	2	4	2	2	2
Dc (Mg/m^3)	2.321	2.567	2.264	1.772	2.304
μ (mm^{-1})	10.090	24.653	21.280	16.419	11.885
F(000)	524	1512	828	396	432
reflns collected	5781	13976	4003	4931	4937
indep. reflns	2810	3266	4003	2043	2677
GOF on F^2	1.033	1.016	1.042	1.165	1.115
R1 (on F_o^2, I > 2σ(I))	0.0201	0.0577	0.0468	0.0638	0.0415
wR2 (on F_o^2, I > 2σ(I))	0.0512	0.1507	0.1253	0.1864	0.1164
R1 (all data)	0.0209	0.0703	0.0537	0.0642	0.0457
wR2 (all data)	0.0517	0.1630	0.1303	0.1866	0.1206

Table 1: X-ray crystal data and structure parameters for compounds **3-5**, **8** and **9**.

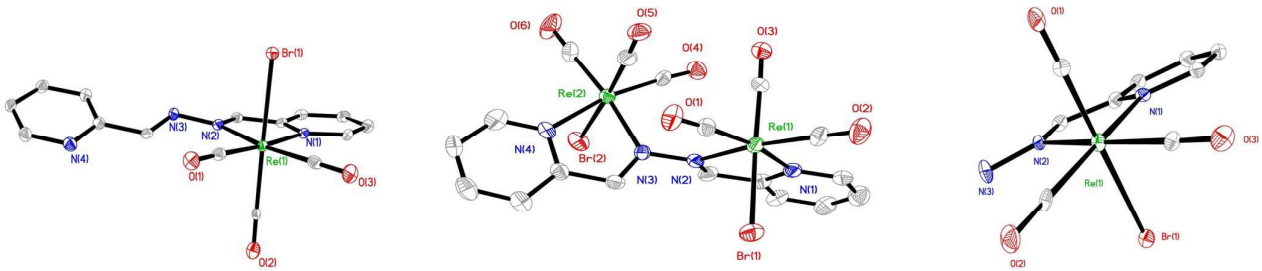

Figure 1. Structures of 3, 5 and 9 with 35% thermal ellipsoids. Hydrogen atoms have been omitted for clarity.

mode observed for bidentate pyridine imine chelates. The structure of the free ligand, **1**, has been previously elucidated[38] and the N-N and C=N bond distances of the dimeric Schiff base unit clearly show single bond (1.413(1) Å) and double bond (1.266(1) Å), characters, respectively. In compounds **2-5**, we observe similar N-N and Schiff base C=N bond distances in the metal-bound chelates, with the only difference being a slight lengthening of the metal-bound C=N double bonds (~1.27-1.29 Å) due to metal-ligand backbonding. These types of complexes are well known and have readily observable spectroscopic features that can be used to establish their identity. [40,43–50] For example, the IR spectra of these compounds exhibit a_1 and e type CO stretching vibrations that result from the facial coordination geometry and local C_{3v} symmetry. In the ^{1}H NMR spectra, the diagnostic CH resonance of the imine confirms the presence of the desired compounds.

Isomerization is clearly seen in the NMR spectra of **4** and **5**, which we have observed previously in similar compounds. Isomerization in **4** and **5** occurs because the halide can be placed on either side of the diimine plane, leading to two stereocenters. Furthermore, as seen in the crystal structures, there are chiral C_2 twists coincident with the N-N bonds. Rotation about the N-N bond is expected to be sterically restricted. For **5**, only one diastereomer was crystallographically observed. For **4**, a single chiral twist conformation was observed, but both enantiomers were observed for each stereocenter. A similar behavior was observed for the *m*-phenylenediimine dimers that we reported previously.[39]

A second, but indirect, way to observe the electronic effects of forming a dimer from two Re diimine compounds via a hydrazine bridge is by UV-visible spectroscopy. Figure 2 shows the spectra of the chloride variants of the monomers (**2** and **8**) as well as the coupled dimeric species, **4**. The spectra of the bromide compounds are nearly identical in appearance (supplementary information). As in other examples of $Re(CO)_3$ diimine complexes, all six compounds exhibit low-energy metal-to-ligand charge transfer (MLCT) bands in the visible region. We can readily determine the identity of these transitions since they are sensitive to the dielectric constant of the solvent. For the monomeric compounds **8** and **9**, the MLCT band is in the UV region of the spectrum at 388 and 393 nm (ε = 3.5 × 10^3 M^{-1} cm^{-1}). With the monomeric compounds **2** and **3**, the additional pyridine imine unit induces a significant red shift of the MLCT absorption band to 437 nm and 433 (ε = 2.6 × 10^2 M^{-1} cm^{-1}), due to the presence (and thus overlap) of the two π systems. For the dimeric systems **4** and **5**, we observe an even greater bathochromic shift to 458 and 470 nm (ε = 6.0 × 10^3 M^{-1} cm^{-1}). The presence of two coupled MLCT transitions result in an approximately 20-30 nm shift in the UV-visible absorbance spectrum; similar shifts have been observed in coupled Ru(II) systems.[51]

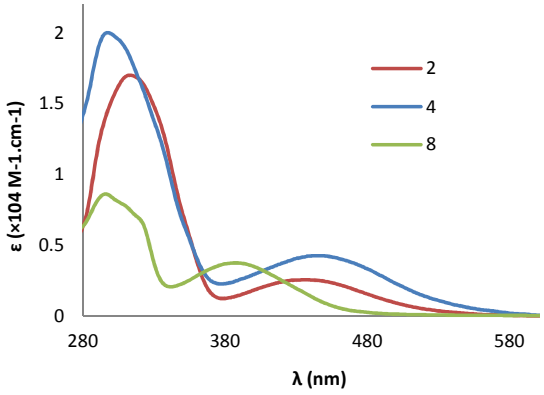

Figure 2: UV-visible spectra for compounds 2, 4 and 8.

We can observe the electronic coupling between the $Re(CO)_3$(pyca) units directly by use of cyclic voltammetry. Figure 3 shows the voltammograms for compounds **4** and **5** (top) versus those from the monometallated compounds **2** and **3**. The scans were carried out in DMF with 0.1 M tetrabutylammonium hexafluorophosphate ($TBAPF_6$) as the electrolyte. These complexes exhibit reversible reductions in the cathodic region, and the electrochemical data is summarized in SI Table S2. Compounds **2** and **3** show a single reversible peak at ~-0.74 V, but for the bimetallic systems **4** and **5**, two reversible reductions are observed. These well-defined reductions are separated by 485 and 482 mV for **4** and **5,** respectively. These separations can be converted to comproportionation constants (K_c) [27,39,51,52] of 1.54 x 10^8 and

1.48 x 10^8 for the two compounds. These values, which correspond to the degree of coupling in **4** and **5**, are on the same order of magnitude as strongly coupled $Ru(bpy)_2$ dimers, such as those that incorporate triazoleate and imidazolate bridges.[46,51] We also investigated the cyclic voltammetry of the monomeric compounds **8** and **9**. The voltammograms, shown in the supplementary information, exhibit irreversible reductions similar to those seen for the corresponding monomers **2** and **3**. The reductions can be assigned as taking place on the diimine ligand regions of these dimers (*vide infra*).

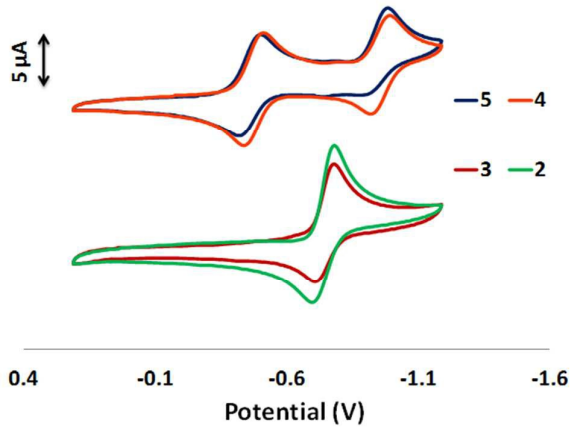

Figure 3: Cyclic voltammograms of monomers and dimers in 0.1 M TBAPF6/DMF at 0.25 V and 10.0 µAV–1 sensitivity versus AgCl.

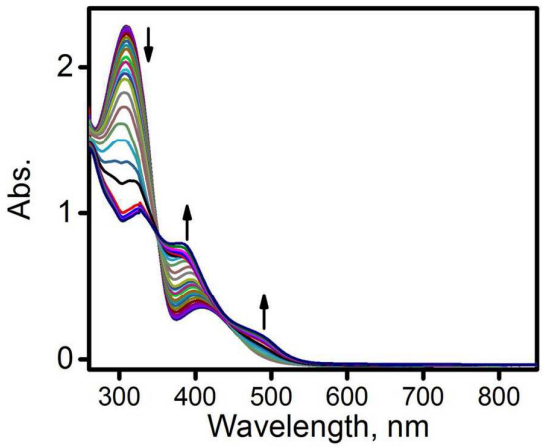

Figure 4 . UV-vis spectra transformation of **2** into **[2]**$^-$ during the first reduction under spectroelectrochemical conditions in DMF/0.3M TBAP system.

In order to evaluate spectroscopic signatures of the reduced species in monomeric complexes **2** and **3** as well as dimeric analogues **4** and **5**, we have conducted spectroelectrochemical experiments in the DMF/0.3M TBAP system. In the case of the monomeric chloro-derivative **2**, reduction under spectroelectorchemical conditions results in an intensity decrease and the low-energy shift of charge-transfer band at 309 nm to 327 nm. In addition, the initial band at 409 nm disappears, while two new bands at 384 and 483 nm appear in the visible region (Figure 4). This reduction is reversible as neutral complex **2** can be regenerated upon oxidation of **[2]**$^-$ (SI Figure S29). Because of the lower stability of Re-Br bond, spectroelectrochemical data for complex **3** are more complicated (Figure 5). Although initial UV-vis spectra transformation during the first reduction process looks similar to those observed in chloro analogue **2**, reoxidation of the electrochemically generated **[3]**$^-$ anion results in a UV-vis spectrum which is different from neutral complex **3**. This spectrum is very similar to pyridine-containing rhenium dimers with a direct Re-Re bond.[53] Transformation of complex **3** into possible dimer was further confirmed by continuous CV experiments (SI Figure S30). Indeed, during such experiments, the initial reduction peak of **3** disappeared, while a new peak appears in the CV curve suggesting transformation of **3** into new species under electrochemical conditions.

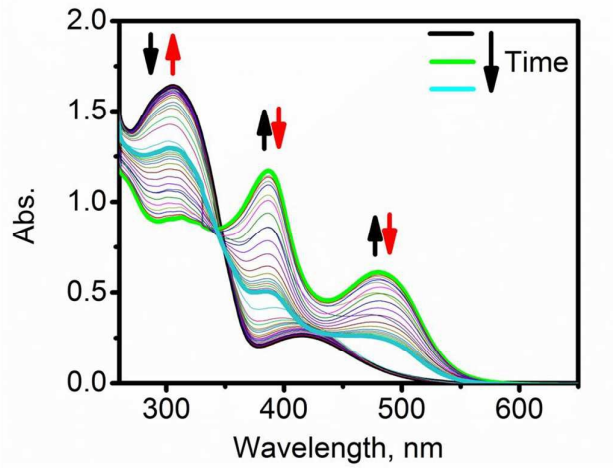

Figure 5. UV-vis spectra transformation of **3** into **[3]**$^-$ followed possible dimerization during the first reduction under spectroelectrochemical conditions in DMF/0.3M TBAP system.

In the case of dimeric complexes **4** and **5**, the first and the second reduction processes are well separated and reversible and thus spectroscopic signatures of all reduced species can be accurately characterized by spectroelectrochemical experiments (Figures 6 and 7). In the case of chlorine-containing dimer **4**, the first, single-electron reduction results in decrease of intensities of 294 and 436 nm bands and appearance of four new bands at 327, 465, 578, and 1130 nm in mixed-valence **[4]**$^-$ (Figure 6). During second single-electron reduction, initial transitions at 327 and 465 nm shift to 331 and 474 nm, while bands at 578 and 1130 nm disappear (Figure 6). Appearance of the broad NIR band at 1130 nm during the first reduction and its disappearance during the second reduction process is clearly indicative of its intra-valence charge-transfer (IVCT) character.

On a qualitative level, spectroelectrochemical transformations of the dibromo complex **5** are similar to those observed in its dichloro analogue **4**. In particular, both initial bands at 282 and 443 nm disappear, while four new transitions at 388, 467, 577, and 1130 nm appear in the spectrum of **[5]**$^-$ during the first reduction process (Figure 7). The NIR band

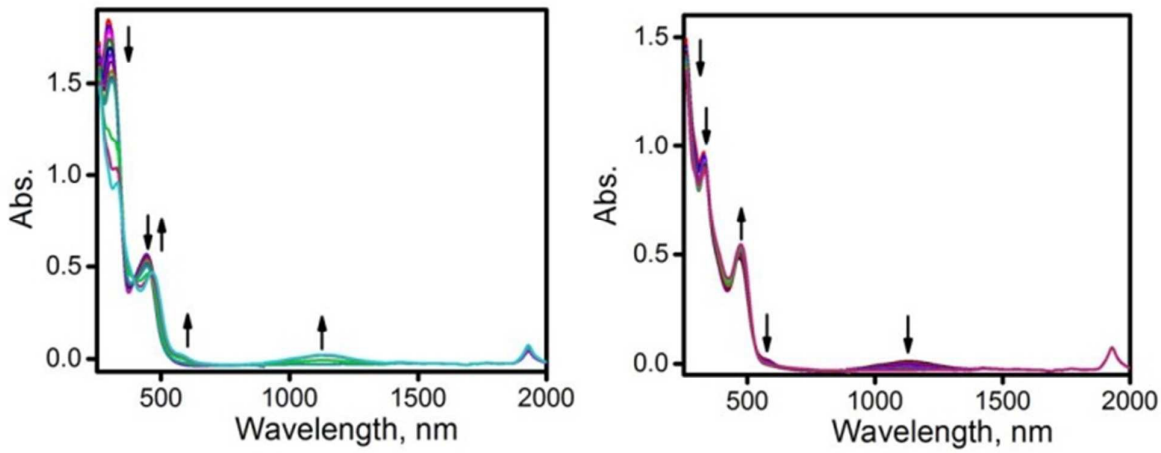

Figure 6. UV-vis spectra transformation of 4 into [4]- during the first reduction (left) and [4]- into [4]2- during the second reduction (right) under spectroelectrochemical conditions in DMF/0.3M TBAP system.

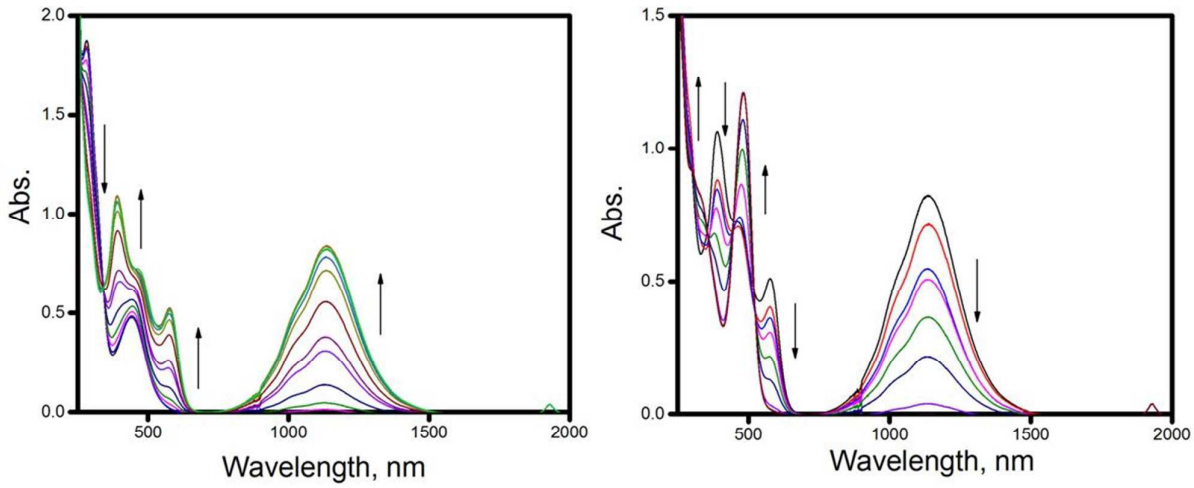

Figure 7. UV-vis spectra transformation of 5 into [5]- during the first reduction (left) and [5]- into [5]2- during the second reduction (right) under spectroelectrochemical condition in DMF/0.3M TBAP system.

observed at 1130 nm in mixed-valence **[5]**$^-$ is significantly more intense than IVCT observed in dichloro analogue **[4]**$^-$ and clearly has an asymmetric shape with a prominent shoulder at ~1020 nm. During second reduction, four bands at 388, 467, 577, and 1130 nm observed in UV-vis-NIR spectrum of **[5]**$^-$ disappear, while two new bands at 355 and 482 nm appear in the spectrum of **[5]**$^{2-}$ (Figure 7). Thus, the asymmetric NIR band in the mixed-valence **[5]**$^-$ can be assigned as IVCT transitions. The monomeric compounds **7** and **8** could not be investigated by spectroelectochemical methods due to the lack of reversibility in their cyclic votammograms. The IVCT bands in the mixed-valence **[4]**$^-$ and **[5]**$^-$ dimers were analyzed in the borders of Hush theory formalism.[54–57] Since the information on the transition dipole moments for intra-ligand IVCT is uncertain, we can only estimate the lower and the upper limits of the coupling matrix element H_{ab}. For IVCT analysis, the crystallographically determined Re-Re distance was used to estimate the upper, and the pyridine(N)-pyridine(N) distance was used to estimate the lower borders of H_{ab}. Band deconvolution analysis of IVCT (SI Figure S31) suggest that both **[4]**$^-$ and **[5]**$^-$ complexes belong to the class III (completely delocalized) systems in Robin-Day classification.[57] The estimated Hab values are 307-420 cm^{-1} for **[4]**$^-$ and 1145-1647 cm^{-1} for **[5]**$^-$ complexes, while estimated Γ = 0.59 (**[4]**$^-$ complex) and 0.63 (**[5]**$^-$ complex).

To elucidate spectroscopic and redox properties of the monomeric complexes **2**, **3**, **7**, and **8** as well as dimers **4** and **5**, we have conducted DFT and TDDFT calculations of all target complexes following procedures similar to those used by us for molybdenum carbonyl compounds.[58] The energy diagram for these compounds is shown in Figure 8, molecular orbital

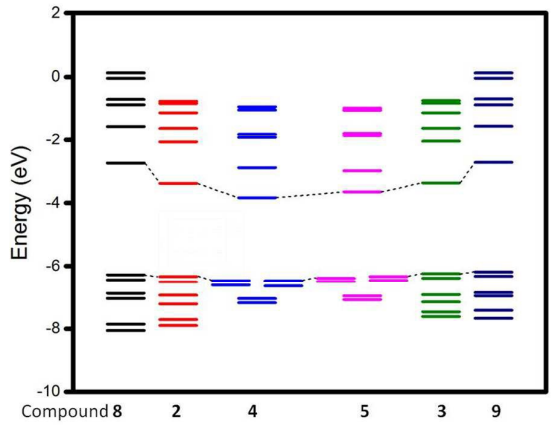

Figure 8. DFT predicted energy diagram for target rhenium compounds.

compositions are listed in the SI, and selected frontier orbitals are shown in Figure 9 and SI Figures S32-37. The DFT-predicted electronic structure of all target compounds is quite similar, which correlate well with their redox properties and UV-vis spectra. First, occupied frontier orbitals are clearly indicative of the low-spin d^6 configuration of the rhenium centers. In particular, in the case of monomeric complexes **2**, **3**, **7**, and **8**, the HOMO, HOMO-1, and HOMO-2 are dominated by rhenium d_{xz}, d_{yz}, and d_{xy} orbital contributions with the first two orbitals being close to each other in energy (Figure 8). For dimeric complexes **4** and **5**, HOMO and HOMO-1 are degenerate and dominated by the equivalent contribution from both rhenium centers forming standard pair of "in" ($d_{xz}+d_{xz}$) and "out" ($d_{xz}-d_{xz}$) of phase combination of d_{xz} orbitals. A similar pattern of "in" and "out" of phase combinations of rhenium d_{yz} and d_{xy} orbitals was also observed for HOMO-2/HOMO-3 and HOMO-4/HOMO-5 pairs, respectively. Again, predominant d_{xz} and d_{yz} orbital combinations are closely spaced, while combinations of d_{xy} orbitals are energetically well separated. In all target complexes, rhenium-centered occupied frontier orbitals follow ligand-based π-MOs and then more stable halogen-centered orbitals (Figure 8). The LUMO and LUMO+1 in all rhenium compounds are predominantly ligand-centered π*-orbitals with the LUMO well-separated in energy (~1 eV) from the LUMO+1. The CO-centered π* orbitals have significantly higher energy than LUMO and LUMO+1. Overall, the electronic structure of the rhenium complexes discussed in this paper is in agreement with the previously reported rhenium-pyridine carbonyls[59,60] and suggestive that the first oxidation should be metal-centered, while the first reduction should be centered on the aromatic ligand, which correlate well with the electro- and spectroelectrochemical data presented above. Thus, associated with the mixed-valence state in **[4]**$^-$ and **[5]**$^-$ the IVCT band represents the intra-ligand rather than metal-to-metal charge transfer and in the absence of information on the transition dipole moments, its analysis should be viewed as only a rough estimate.

In order to improve tentative assignments in the UV-vis spectra of all rhenium complexes, we have conducted a set of TDDFT calculations on these systems. TDDFT predicted energies of all complexes are in reasonable agreement with the experimental data (Figure 10). In the case of all four mononuclear rhenium complexes, two major regions of the spectra were predicted by TDDFT calculations. The low-energy region is described by the MLCT transitions dominated by the intense band mostly originating from HOMO-1 → LUMO excitation. The UV region of the spectra has a major contribution from intra-ligand π–π* excitations. Because of the presence of a larger number of rhenium-centered occupied orbitals in dimeric complexes **4** and **5**, TDDFT predicted UV-vis spectra of these complexes have a larger number of excited states, although qualitative picture remains the same: low-energy transitions have predominantly MLCT character, while UV region is dominated by the intra-ligand π–π* excitations.

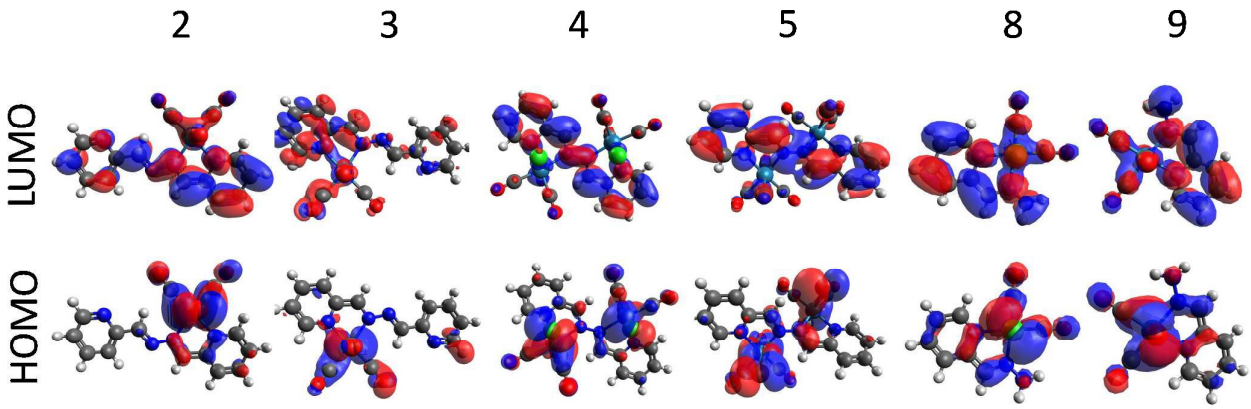

Figure 9. DFT predicted frontier MOs for target rhenium compounds.

Conclusions

In conclusion, dimeric $Re(CO)_3$ pyridine imine complexes can be readily generated by reaction of ligand **1** with $Re(CO)_5X$ precursors. Both monomeric and dimeric species can be generated by use of alcoholic solvents with different boiling points. Simple monomeric compounds (those with ligand **1** and only one equivalent of metal and monomeric Schiff base complexes) can also be generated and provide useful controls for understanding the electronic interactions between the two halves of the dimeric compounds **4** and **5**. We observe strong coupling in compounds **4** and **5** as evidenced by cyclic voltammetry as well as UV-visible spectroscopy. Spectroelectrochemical measurements support these conclusions with the observation of IVCT bands in **4** and **5** upon single electron reduction. DFT and TDDFT calculations indicate that the reductions are ligand-centered, which support intra-ligand transitions for the IVCT bands We are continuing our work on $Re(CO)_3$ dimeric and polymeric systems, and are investigating their properties as possible components of photonic materials.

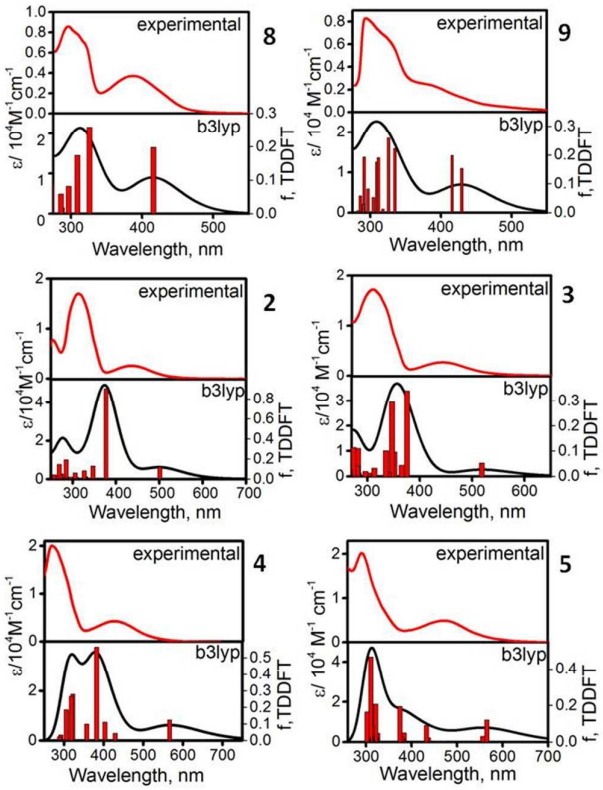

Figure 10. TDDFT predicted UV-vis spectra for target rhenium compounds.

Acknowledgements

RSH would like to thank the Petroleum Research Fund (51085-UR3) for financial support of this research. CJZ would like to acknowledge the University of Akron for support of this work as well as and the National Science Foundation (CHE-9977144) for funds used to purchase the diffractometer used in this work. Generous support from Minnesota Supercomputing Institute for VNN is greatly appreciated.

References

1 A. Juris, S. Campagna, I. Bidd, J.M. Lehn, R. Ziessel, *Inorg. Chem.* 1988, **27**, 4007–4011.
2 M. Mauro, C.-H. Yang, C.-Y. Shin, M. Panigati, C.-H. Chang, G. D'Alfonso, L. De Cola, L. *Adv. Mater.* 2012, **24**, 2054–2058.
3 G. Pereiras-Gabián, E. M. Vázquez-López, U. Abram, *Zeit. Anorg. Allg. Chem.* 2004, **630**, 1665–1670.
4 T. Rajendran, B. Manimaran, F.-Y. Lee, G.-H. Lee, S.-M. Peng, C. M. Wang, K.-L. Lu, *Inorg. Chem.* 2000, **39**, 2016–2017.
5 Y.-H. Tseng, D. Bhattacharya, S.-M. Lin, P. Thanasekaran, J.-Y. Wu, L.-W. Lee, M. Sathiyendiran, M.-L. Ho, M.-W. Chung, K.-C. Hsu, P.-T. Chou, K.-L. Lu, *Inorg. Chem.* 2010, **49**, 6805–6807.
6 E. Ferri, D. Donghi, M. Panigati, G. Prencipe, L. D'Alfonso, I. Zanoni, C. Baldoli, S. Maiorana, G. D'Alfonso, E. Licandro, *Chem. Commun.* 2010, **46**, 6255–6257.
7 M. Panigati, M. Mauro, D. Donghi, P. Mercandelli, P. Mussini, L. De Cola, G. D'Alfonso, *Coord. Chem. Rev.* 2012, **256**, 1621–1643.
8 J. A. Baiano, D.L. Carlson, G.M. Wolosh, D.E. DeJesus, C.F. Knowles, E.G. Szabo, W.R. Murphy, *Inorg. Chem.* 1990, **29**, 2327–2332.
9 P.J. Blower, J.R. Dilworth, J.P. Hutchinson, J. Zubieta, *Transit. Met. Chem.* 1982, **7**, 354–355.
10 T. Tabeya, M. Abe, A. Mitani, K. Tsuge, Y. Sasaki, *J. Nucl. Radiochem. Sci.* 2005, **6**, 157–159.
11 J. W. M. Van Outersterp, F. Hartl, D. J. Stufkens, *Organometallics* 1995, **14**, 3303–3310.
12 A. Vogler, J. Kisslinger, *Inorg. Chim. Acta* 1986, **115**, 193–196.
13 V. W. Yam, K. M. Wong, K. Cheung, *Organometallics* 1997, **16**, 1729–1734.
14 B. J. Yoblinski, M. Stathis, T.F. Guarr, *Inorg. Chem.* 1992, **31**, 5–10.
15 S. Van Wallendael, R. J. Shaver, D. P. Rillema, B. J. Yoblinski, M. Stathis, T.F. Guarr, *Inorg. Chem.* 1990, **29**, 1761–1767.
16 C. M. Álvarez, R. García-Rodríguez, J. M. Martín-Alvarez, D. Miguel, J. A. Turiel, *Inorg. Chem.* 2012, **51**, 3938–3940.
17 G. Böhm, K. Wieghardt, B. Nuber, J. Weiss, J. *Angew. Chem. Int. Ed. Engl.* 1990, **29**, 787–790.
18 C. Bruckmeier, M. W. Lehenmeier, R. Reithmeier, B. Rieger, J. Herranz, C. Kavakli, *Dalton Trans.* 2012, **41**, 5026–5037.
19 J. A. Cabeza, A. Llamazares, V. Riera, R. Trivedi, F. Grepioni, *Organometallics* 1998, **17**, 5580–5585.
20 J. Granifo, *Polyhedron* 1999, **18**, 1061–1066.
21 H. Qayyum, R.S. Herrick, C.J. Ziegler, *Dalton Trans.* 2011, **40**, 7442–7445.
22 E. Spaltenstein, J. M. Mayer, *J. Am. Chem. Soc.* 1991, **113**, 7744–7753.
23 J. W. M. Van Outersterp, D. J. Stufkens, A. Vlcek, *Inorg. Chem.* 1995, **34**, 5183–5194.
24 F. P. A. Johnson, M. W. George, F. Hartl, J. J. Turner, J. J. *Organometallics* 1996, **15**, 3374–3387.
25 G. J. Stor, F. Hartl, J. W. M. van Outersterp, D. J. Stufkens, *Organometallics* 1995, **14**, 1115–1131.
26 B. D. Rossenaar, F. Hartl, D. J. Stufkens, *Inorg. Chem.* 1996, **35**, 6194–6203.
27 P. J. Ball, T. R. Shtoyko, J. A. Krause Bauer, W. J. Oldham, W. B. Connick, *Inorg. Chem.* 2004, **43**, 622–632.
28 P. T. Kissinger, W. Lafayette, W. R. Heineman, *J. Chem. Educ.* 1983, **60**, 702–706.
29 A. D. Le, L Yu, *J. Electrochem. Soc.* 2011, **158**, F10.

30 N G. Connelly, W. E. Geiger, *Chem. Rev.* 1996, **96**, 877–910.
31 A. D. Becke, *J. Chem. Phys.* 1993, **98**, 5648.
32 C. Lee, W. Yang, R. G. Parr, *Phys. Rev. B* 1988, **37**, 785–789.
33 A. Canal Neto, F. E. Jorge, *Chem. Phys. Lett.* 2013, **582**, 158–162.
34 A. D. McLean, S. G. Chandler, *J. Chem. Phys.* 1980, **72**, 5639.
35 J. Tomasi, B. Mennucci, R. Cammi, *Chem. Rev.* 2005, **105**, 2999–3093.
36 M. J. M.Frisch, G. W. Trucks, H. B. Schlegel, G. E. Scuseria, et al. Gaussian 09, 2009.
37 A. L. Tenderholt, QMForge.
38 E. C. Kesslen, W.B. Euler, B. M. Foxman, *Chem. Mater.* 1999, **11**, 336–340.
39 A. Hasheminasab, J. T. Engle, J. Bass, R. S. Herrick, C. J. Ziegler, *Eur. J. Inorg. Chem.* 2014, **2014**, 2643–2652.
40 N. M. Shavaleev, Z. R. Bell, G. Accorsi, M. D. Ward, *Inorg. Chim. Acta* 2003, **351**, 159–166.
41 R. Costa, K. Chanawanno, J. T. Engle, B. Baroody, R. S. Herrick, C. J. Ziegler, *J. Organomet. Chem.* 2013, **734**, 25–31.
42 L. A. García-Escudero, D. Miguel J. A. Turiel, *J. Organomet. Chem.* 2006, **691**, 3434–3444.
43 D. A. Edwards, G. M. Hoskins, M. F. Mahon, K. C. Malloy, G. R. G. Rudolph, *Polyhedron* 1998, **17**, 2321–2326.
44 W. J. Stratton, D. H. Busch, *J. Am. Chem. Soc.* 1960, **82**, 4834–4839.
45 W. J. Stratton, D. H. Busch, *J. Am. Chem. Soc.* 1958, **80**, 3191–3195.
46 P. Cai, M. Li, C.-Y. Duan, F. Lu, D. Guo, Q.-J. Meng, *New J. Chem.* 2005, **29**, 1011.
47 M. Chandra, A. N. Sahay, S. M. Mobin, D. S. Pandey, *J. Organomet. Chem.* 2002, **658**, 43–49.
48 V. Chandrasekhar, T. Hajra, J. K. Bera, S. M. W. Rahaman, N. Satumtira, O. Elbjeirami, M. A. Omary, *Inorg. Chem.* 2012, **51**, 1319–1329.
49 R. Karmakar, C. R. Choudhury, S. R. Batten, S. Mitra, *J. Mol. Struct.* 2007, **826**, 75–81.
50 G. Mahmoudi, A. Morsali, *Cryst. Growth Des.* 2008, **8**, 391–394.
51 D. E. Richardson, H. Taube, *J. Am. Chem. Soc.* 1983, **105**, 40–51.
52 D. M. D'Alessandro, F. R. Keene, *Dalton Trans.* 2004, 3950–3954.
53 D. L. Morse, M. S. Wrighton, *J. Am. Chem. Soc.* 1976, **98**, 3931–3934.
54 N. S. Hush, *Prog. Inorg. Chem.* 1967, **8**, 391–444.
55 C. Creutz, *Progr. Inorg. Chem.* 1983, **30**, 1–73.
56 N. S. Hush, *Coord. Chem. Rev.* 1985, **64**, 135–157.
57 M. B. Robin, P. Day, *Adv. Inorg. Chem. Radiochem.* 1968, **10**, 247–422.
58 V. N. Nemykin, J. G. Olsen, E. Perera, P. Basu, P. *Inorg. Chem.* 2006, **45**, 3557–3568.
59 A. Drozdz, M. Bubrin, J. Fiedler, S. Záliš, W. Kaim, W. *Dalton Trans.* 2012, **41**, 1013–1019.
60 R. Heydová, E. Gindensperger, R. Romano, J. Sýkora, A. Vlček, S. Záliš, C. Daniel, *J. Phys. Chem. A* 2012, **116**, 11319–11329.